INTENSITY NORMALIZATION BY INCIDENCE ANGLE AND RANGE OF FULL-WAVEFORM LIDAR DATA

H. Gross, B. Jutzi, U. Thoennessen

FGAN-FOM, Research Institute for Optronics and Pattern Recognition Gutleuthausstraße 1, 76275 Ettlingen, Germany - (gross,jutzi,thoe)@fom.fgan.de

Commission IV, WG IV/3

KEY WORDS: Laser Data, Full-Waveform, Point Clouds, Intensity, Normalization, Covariance, Eigenvalues, Lambertian Law.

ABSTRACT:

The analysis of LIDAR data to extract surface features is of great interest in photogrammetric research. Our investigations show that the same material of a surfaces (e.g. gabled roof) yields to different measured values for the intensity due to the incidence angle. These values are strongly correlated to the incidence angle of the laser beam on the surface. Therefore we improve the value of the intensity by considering the incidence angle derived by the sensor and object position as well as its surface orientation. The surface orientation is estimated by the eigenvectors of the covariance matrix including all object points inside a close environment. The adaptation of vegetation areas is disregarded. After these improvements the intensity does no longer depend on the incidence angle but may be influenced by the material of the object surface only. The surface characteristic depends on the used wavelength. A measurement campaign was carried out to investigate the influences of the incidence angle on the measured intensity. By considering the incidence angle and the distance between sensor and object the laser data captured from different flight paths (data stripes) can be successfully fused. In our experiments it could be shown that the normalization of the intensity for the investigated areas are improved.

1. INTRODUCTION

The high potential of laser scanning data for the automatic generation of 3d models has been demonstrated in the past (Brenner et al., 2001; Geibel & Stilla, 2000; Gross et al., 2005). Spaceborne, airborne as well as terrestrial laser scanning systems allow a direct and illumination-independent measurement from 3d objects in a fast, contact free and accurate way.

The latest developments of commercial airborne laser scanners allow recording the waveform of the backscattered laser pulse, namely the LEICA ALS-50II, OPTECH ALTM 3100, TOPEYE MK II, and TOPOSYS HARRIER 56. The latter one is based on the RIEGL LMS-Q560. In addition to the mentioned airborne laser scanners, the prototype of the terrestrial laser scanning system ECHIDNA (Lovell et al., 2003) has the opportunity to capture the waveform too.

To interpret the received waveform of the backscattered laser pulse, a fundamental understanding of the physical background of pulse propagation and surface interaction is important. The waveform includes imlicit information about different features like the range, elevation variations, and reflectance of the illuminated surface based on the inclination between the divergent laser beam and object plane. Additonally the received waveform depends on the wavelength of the emitted laser light.
The waveform of each pulse is described by a series of range values combined with amplitude values and can be approximated by one or more parameterized Gaussian curves (Hofton et al., 2000; Persson et al., 2005; Wagner et al., 2006). Due to this approximation the temporal position, width and amplitude caused by the object surfaces are estimated (Jutzi & Stilla, 2006). With these parameters the geometry and the reflectance of the illuminated surface can be investigated.

The material reflectance features from the measured data mainly depends on the incidence angle of the beam on the surface, the surface properties and the laser wavelength (Jelalian, 1992).
In the terminology of laser scanning the reflectance is widely used as synonym for the amplitude or energy, where the energy of each pulse is the integral over its waveform. For a Gaussian pulse this can be simplified and approximated by the product of amplitude and width. Beside this the term intensity is used for the amplitude or energy.

Various studies about surface reflectance and the related intensity have been published in the literature:

- Höfle & Pfeifer (2007) showed a data and a model-driven method for correcting the intensity for specific influences. The corrected intensity is successfully used to generate intensity images with lower systematic errors.
- Katzenbeisser (2003) introduced for flat surfaces that the measured intensity provide a reasonable mean for the reflectance, if the measured intensity is corrected by the known distance.
- Kukko et al. (2007) measured for various urban materials the dependency of the intensity from the incidence angle.
- Pfeifer et al. (2007) studied the influence on the intensity for surfaces with varying incidence angles, known reflectance and scattering characteristics. It is shown that the range dependent inverse-square model might be insufficient to estimate the accurate intensity.
- Reshetyuk (2006) investigated for various materials the surface reflectance and its influences on the measured range and intensity.

For applications, where the intensity is of interest, a normalization based on the incidence angle is needed. The variation of the incidence angle increases if data from several flights with different paths are fused.To give an example a RGB-image together with the corresponding intensity values from two different flights is visualized in

Figure 1. The viewing direction of the sensor system is depicted by a black arrow. The area of interest is the gabled roof. The roof area orientated towards the sensor systems delivers higher intensity values, while the turn away roof area delivers significant smaller intensity values.

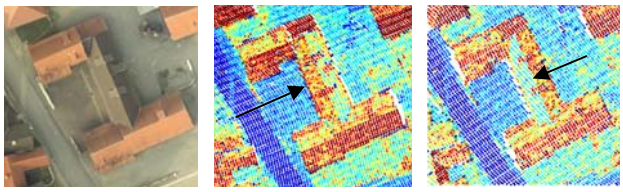

a b c

Figure 1: Dependency of the intensity from the incidence angle:
a) RGB image,
b) Intensity values of flight 3,
c) Intensity values of flight 4.

These from the waveform estimated values are strongly correlated to the incidence angle of the laser beam on the surface. Therefore we propose to normalize the value of the intensity by considering the incidence angle derived by the sensor and object position as well as its surface orientation.

In Section 2 a brief description of the used full-waveform data is given. Further we introduce the physical constraints, the required normalization step, and the methodology for calculation of the normal vectors of the surfaces based on the covariance matrix and the resulting incidence angle. The description of the scene and the gathered data is presented in Section 3. In Section 4 homogenous test regions are selected for the assessment of the normalization. The results including a presentation of the values before and after the normalization are demonstrated in Section 5. Finally the used formula and derived results are discussed.

2. METHOLOGY

2.1 Terminology of Full-Waveform Data

By the full-waveform laser data acquisition for each beam the total number of detected backscattered pulses is known and is assigned to the corresponding echoes. Each echo is described by a point with its 3d coordinate, signal amplitude a , and signal width w at full-width-at-half-maximum derived from the Gaussian approximation. Additionally the 3d coordinate of the sensor position is available.

The shape of the received waveform depends on the illuminated surface area, especially on the material, reflectance of the surface and the inclination angle between the surface normal and the laser beam direction. The typical surface attributes which can be extracted from a waveform are range, elevation variation, and reflectance corresponding to the waveform features: time, width and amplitude.

The intensity (energy) is estimated by the width multiplied with the amplitude of the Gaussian approximation and modified by the range between sensor and object with respect to the extinction by the air. It describes the reflectance influenced by geometry and material of the object at this point. For each particular echo caused by partially illuminated object surfaces we receive an own intensity value.

2.2 Physical Constraints

For data acquisition a monostatic laser scanning system is used. The received energy $E_r = c \cdot a \cdot w$ is calculated from amplitude and width of the received signal approximation. The factor c is constant and has therefore no influence for our consideration. Considering an energy balance it depends on the transmitted energy E_t , the distance R to the object surface, and the incidence angle ϑ, which is given by the angle between the transmitter direction and the surface normal vector

$$E_r = E_t \frac{C_t C_r T^2(R) \cos(\vartheta)}{R^2} f(c_s), \qquad (1)$$

where C_t and C_r are constant terms of the transmitter and the receiver (Kamermann, 1993; Pfeifer et al., 2007). The atmospheric attenuation along the way from the transmitter to the object and return to the receiver is describes by $T^2(R) = e^{-2\alpha R}$. Let $f(c_s)$ entail all other influences like surface material and local surface geometry. This formula is valid for objects with larger size than the footprint of the laser beam. All constant terms may be ignored because at this point we are interested only on the behaviour of the received intensity. Knowing the received amplitude and width of the signal a range corrected intensity is calculated to

$$I_R = C_1 \cdot a \cdot w \cdot T^{-2}(R) \cdot R^2, \qquad (2)$$

where C_1 may be any arbitrary constant. This intensity I_R does not dependent on the distance R anymore. For homogenous regions, cf. the following sections, this formula delivers value differences less than 5% in comparison with using a mean distance. This is only valid for data captured at a single flight path. I_R is influenced by the material properties and the incidence angle.For all points with high planarity we normalized the measured intensity additionally by $I = I_R / \cos(\vartheta)$ considering the incidence angle. The illumination direction $\bar{e}_t$ is calculated from the sensor to the object position. The normal vector of an object surface is determined by the evaluation of the covariance matrix, cf. Section 2.3, with respect to the smallest eigenvalue λ_3 and its eigenvector $\bar{e}_3$. With this normalized vectors we calculate the required divisor by $\cos(\vartheta) = |\bar{e}_t \circ \bar{e}_3|$. These correction steps remove known influences from the measured intensity. Therefore the normalized intensity I depends for the used wavelength on the material properties only. The influence of speckle effects is neglected.

2.3 Covariance and Normal Vectors of Object Surfaces

For each point in the data set we consider all points in a small spherical neighborhood, calculate the covariance matrix and the eigenvalues and eigenvectors (Gross & Thoennessen, 2006). These can be used to detect plane surfaces.
The eigenvalues λ_i and eigenvectors $\vec{e}_i$ with $i = 1,2,3$ of the symmetrical matrix deliver additional features for each point. The eigenvalues are invariant concerning rotation of the coordinate system. For the decision, whether a point belongs to a planar surface West et al. (2004) propose the structure tensor planarity $= \frac{\lambda_2 - \lambda_3}{\lambda_1}$ and $\vec{e}_3$ is the normal vector of the planes.

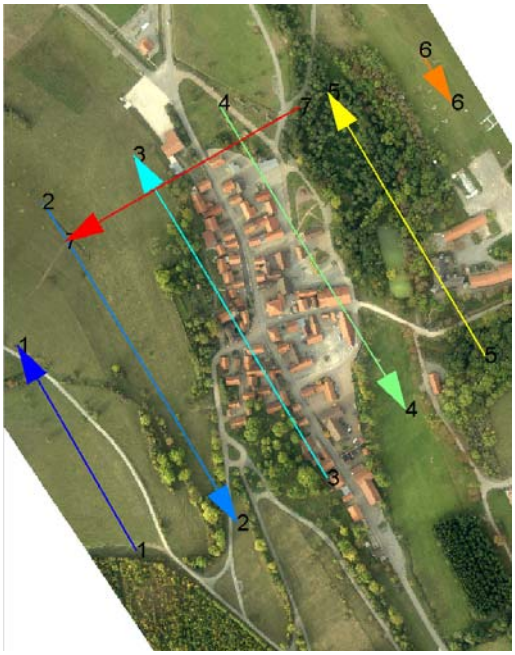

Figure 2. Overlay of flight paths on an airborne image.

3. TEST SCENE

A measurement campaign was carried out to investigate the influences of the incidence angle on the measured intensity. For the scene an urban area including buildings, streets, grassland, and trees was selected. The data was gathered with the RIEGL LMS-Q560. Several flights with different trajectories to gain overlapping stripes were performed. The entire scene is covered by a high point density of about 13 points per square meter.
In
Figure 2 the different flight paths are drawn. Six flight paths are parallel and oriented nearly along the valley starting from the west side. Flight path seven crosses the other.

Figure 3a shows each measured point coloured by its height. A first impression of the measured intensity is given by Figure 3b.The influences of the flight path respectively the local incidence angle on the intensity values is shown in

Figure 4. The trajectories 2 to 5 have about 330m distance. If the laser beam hits an object only partially, e.g. a roof edge, the resulting intensity decreases (Jutzi et al., 2005). Already a small offset (116m) between the two flight path trajectories 2 and 3, yields essential different incidence angles like presented in Figure 4a and b. The square building with four roof planes on the left border of the image (

Figure 4a-c) demonstrates, that small angles are given, if the plane normal vectors point to the sensor. Larger ones can be observed, if the normal vector is orientated to the opposite direction.

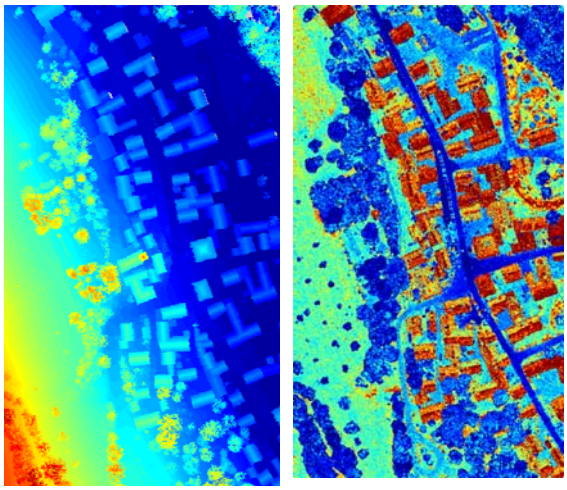

a b

Figure 3. Point cloud for an area of 200x350m²: a) coloured by height values, b) coloured by intensity values.

3.1 Influence of the flight paths on the incidence angle

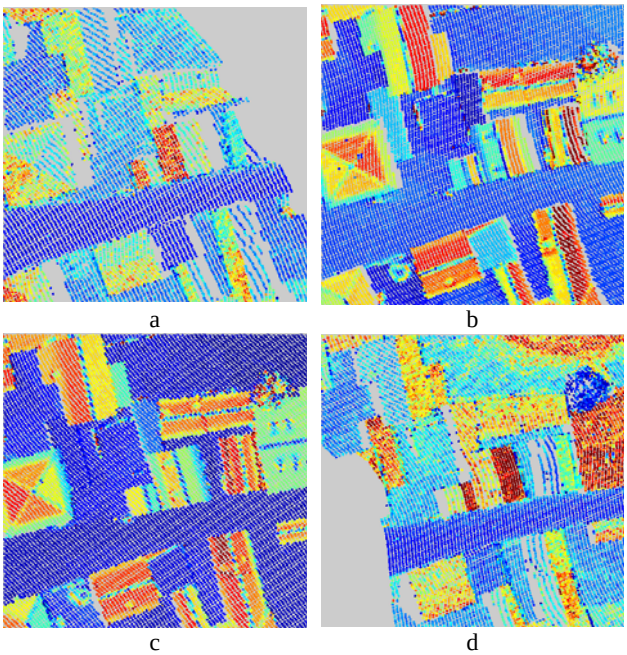

a b

c d

Figure 4. Influence of the incidence angles on the intensity:

a) flight path 2, b) flight path 3, c) flight path 4,
d) flight path 5.

During flight 2 (Figure 4a) we look from the west side onto the roof planes (saddle roof) of the buildings in the middle of the image. Therefore measured intensity values on the roof planes pointing to west are higher than for the roof planes pointing to east. For flight 5 (d) we are looking from east onto the same

roof planes and hence the intensity values are higher for the eastern planes and lower for the west ones.

3.2 Point Density

The calculation of the incidence angle and the planarity is based on the determination of the covariance for each point by including all neighbour points inside a sphere with predefined radius. For a radius of 1m we may get about 30.5 points as average, if we include all flights. Flight 3 delivers as average only 8.8 points. Increasing the radius by factor 2 we get the average value of 120.6 points per sphere and all flights included, where 33.6 points are originated from flight 3. Due to the small size of the roof regions we select a radius of 1m to avoid too much disturbance for the points near the border of the object planes. The inhomogeneous and anisotropic point distribution causes a reduction of the planarity value and raises its standard deviation even if the 3rd eigenvalue equals to zero, because the eigenvalues belonging to both eigenvectors parallel to the plane may differ, as discussed by Gross (2006). Investigations concerning the quality of the point position are also presented by Bae et al. (2005).

4. SELECTION OF HOMOGENEOUS REGIONS

For the assessment of the adapted intensity I we prefer regions with different orientations but homogenous surface reflectance to separate the influences of the incidence angle and material effects. The roof planes within our scene cover a large band of possible incidence angles but most of them have same tiles. The selected regions contain the same material but varying angle vs. flight direction and the direction of the laser beam. Each roof plane is labeled by a region number.

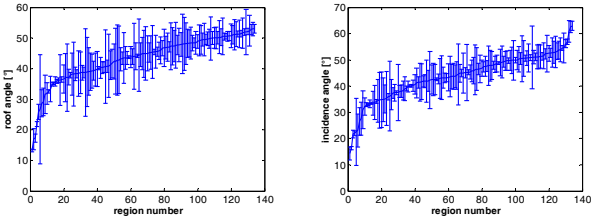

a b

Figure 5. Angles [°] of flight 3 for all selected plane regions sorted by the mean angle together with its standard deviation: a) slope of roofs, b) incidence angles.

This selection includes a wide range concerning the off nadir angle for the laser beam. The variation inside the regions is small because the regions are small in comparison with the distance to the sensor. The slope angle of the roof planes (

Figure 5a) encloses a few nearly flat roofs but also steeper roofs up to 50°. For each point of the point cloud inside the region the slope angle is calculated based on the eigenvector of the smallest eigenvalue. Therefore the data set encloses regions with small and height variations of the slope angle, which may be influenced by small objects on top of the roofs.The planarity yields high values for planes objects, where the mean value varies from 0.67 to 0.83. Due to noise and disturbing small object parts, higher values could not be achieved. The standard deviation inside the regions varies from 0.06 to 0.13, which indicates, that the planes are not exactly planar and does not show the same roughness. The incidence angle (

Figure 5b) varies from 2° to 68° with a mean value from 44°. The standard deviation delivers values from 0.5° to 12° with a mean value from 4°. Inside a region the variation of the incidence angle is small. The distances R between sensor and object surface varies from 429m to 449m with a mean standard deviation of 1m.

5. RESULTS

For the selected regions the given intensity is normalized by division with the cosine of the incidence angle. By this division the normalized intensity value increases compared to the original one. Therefore we use the mean value $\mu(x)$ and the standard deviation $\sigma(x)$ for the calculation of the variation coefficient $V_c(x) = \sigma(x)/\mu(x)$. This coefficient is scale invariant and regards the dependency of the standard deviation from the intensity as presented by Pfeifer et al. (2007).

5.1 Global Consideration Over all Regions in Common

Mean value and standard deviation of the variation coefficient over all roof regions with nearly the same material

$$\mu(V_c(region)) \quad \text{and} \quad \sigma(V_c(region))$$

are determined and written in

Table 1. Considering only flight 3 or 4 there are no significant value modifications, but including flight 3 and 4 together the normalization delivers an essentially smaller standard deviation. The variance of the incidence angle for each region increases, if data from more than one flight are used. In the last column of

Table 1 we see the corresponding values by regarding all flights. In this case we get a good improvement for the normalized intensity.

Flights		3	4	3-4	1-7
before normali-zation	$\mu(V_c)$	0.145	0.142	0.162	0.189
	$\sigma(V_c)$	0.030	0.027	0.028	0.039
after normali-zation	$\mu(V_c)$	0.145	0.144	0.150	0.161
	$\sigma(V_c)$	0.027	0.023	0.023	0.023

Table 1. Mean value and standard deviation for different flight situation data sets before and after normalization.

5.2 Consideration of each region separately

For an assessment the ratio of the variation coefficient $R_V(region) = V_{c,after}(region)/V_{c,before}(region)$ for all selected regions after vs. regions before normalization are calculated. The sorted ratios are drawn in Figure 6.

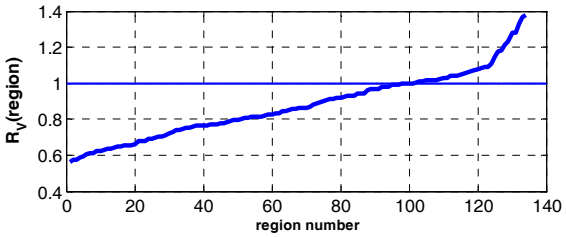

Figure 6. Sorted ratios of the variation coefficients after vs. before normalization of the intensity.

About 75% of the selected regions become values below 1.0 meaning the new coefficient is better (smaller) than the previous one. In some cases with higher values than 1.0 the regions contain chimney and dormer windows. On the other side we can not be sure, that the borders of the regions are well defined inside a homogeneous area.

5.3 Visualization of the Normalized Data

The intensity improvements are demonstrated by the following figures showing the intensity values before and after the normalization by the incidence angle. For comparison reasons the colours dark blue and dark red are bounded to the thresholds 5% respectively 95% as lower and upper percentiles of the intensity. The normalized intensity reflects higher intensities without large variations for the roof planes but lower values for points near the ridge, where the planarity is not given. The results for a pyramidal roof including four planes are shown by

Figure 4. The original data shows higher values for the south-west planes than for the north-east ones caused by the flight paths and directions (

Figure 2). In the normalized data all four planes have same intensity values and appear homogeneous. A building composed by several parts with different orientation is given in Figure 7. The original data demonstrates again the dependency of the intensity from the incidence angle. By the normalization this dependency is compensated and again the intensity is adapted.

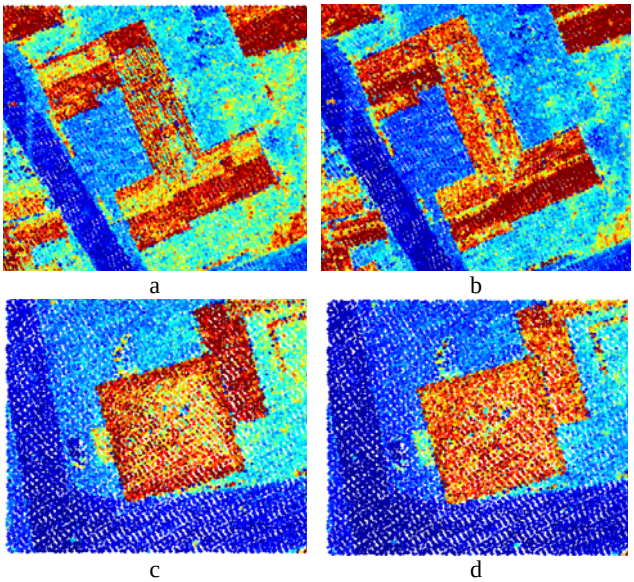

Figure 7.Intensity data for different orientated roofs.
Gabled roofs: a) original, b) normalized, Pyramidal roof: c) original, d) normalized.

Obviously the effect of intensity normalization is not as much evident for street regions. The variance of the incidence angle is much smaller than for roofs.

5.4 Intensity of a region with different geometry

For the investigation on the intensity within a region, we select two neighboured planes with the same material and the same gradient direction but varying roof slopes. The intensity values for all points inside this region are visualized in

Figure 8 coloured by the flight number.

Figure 8a shows the original data and the approximating cosine curve as black line. In b the normalized intensity values are scaled in such a way, that the mean value, drawn by a black line, remains the same as before. The correspondence between flight number and colour is depicted in top of

Figure 8b. There exist no points from the flights 1 and 6.

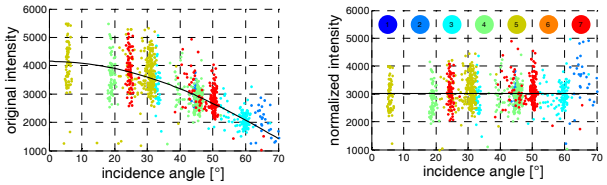

Figure 8. Intensity values vs. incidence angle coloured by the flight number: a) original data, b) normalized data.

From all other flights we observe always two cluster caused by the roof of the main building and an extension of it with different normal vector. Both belong to the same region. To give an example, for flight 7 we have incidence angles for 25° and 50° and for flight 5 for 6° and 31°, as examples. The total number of points inside this region is 1055. The number of points belonging to the different flights can be seen in

Table 2. The ratio of the variation coefficients for this region is $R_V = 0.68$, subsequently the normalized intensity value is 32% better than the original one.

Flight	2	3	4	5	7
Points	77	156	259	308	255

Table 2. Number of points in the selected region measured by the corresponding flights.

Based on the high variation of the intensity before and after normalization by the cosine law, we suppose, that the influence of surface effects like the kind of material or local geometry can not be ignored for man-made surfaces. In contrast to this Lutz et al. (2003) observe high variations for the intensity values for natural materials.

5.5 Adaptation of the Lambertian Law

The reflectance may not be always in accordance with the Lambertian law. Adapting the Lambertian cosine law and trying to minimize the variation coefficient for each region separately by varying the power p of $\cos(\vartheta)^p$ the best values are achieved for powers between 0.5 and 1.1 (Figure 9).

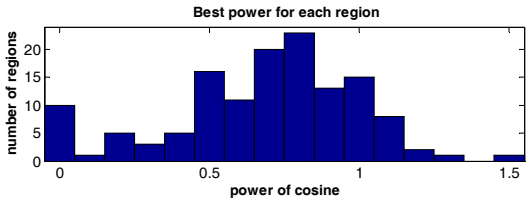

Figure 9. Best values for the power of the cosine.

This figure shows the number of regions among the selected ones together with its power delivering the smallest coefficient. For $p = 0.75$ we get a common minimum for all regions meaning the sum of the variation coefficient over all regions is minimal for this power. This power may depend on the material.

6. DISCUSSION AND CONCLUSION

The measured LIDAR intensity values depend on the distance between sensor and object as well as for the incidence angle defined by the beam direction and the normal vector of an object surface. The normalization of the intensity by considering the object distance in a typical urban area yields only small modifications below 5%. Larger effects on the intensity are caused by the incidence angle.

Investigations on full-waveform laser data are realized, where for each measured point of the point cloud the amplitude and width values are available. In a first step the range modified intensity, influenced by the distance between sensor and object surface, concerning the geometry and the extinction of the signal is evaluated. In a second step we divide the new intensity value by cosine of the incidence angle following the Lambertian law.

All processing steps are done on aerial laser elevation data of a urban area including differences in the distance and a large interval for the incidence angle, especially if we include more than only a single flight. Including all flight we get about 9.6 points/m². The distribution of the points implies high variances for the locally calculated planarity even if all points fall in a plane.

For assessment of the normalized intensity values we have selected nearly homogenous regions interactively. The variation coefficient is selected as measure for the comparison of the values before and after normalization. Mean and standard deviation of this measure over all regions decreases by the normalization, especially if all flight are included. For about 75% of the regions we get better values, for the other region we may have disturbances on the roofs like a chimney. The same process is evaluated also for streets parts but is not discussed here. A detailed discussion of the intensity behaviour inside a region demonstrates a high variance even for constant incidence angle. This may caused by material features or local surface effects. Nevertheless normalization in common with the Lambertian law is useful. A modification of this law can produce a better result with respect to the variation coefficient and for the situations used her. There is no extrapolation test for other material available as yet.

Removing well known influences on the intensity value separates different effects and supports the understanding of the data for further analysis.

REFERENCES

Bae, K., Belton, B., Lichti, D., 2005. A Framework for Position Uncertainty of Unorganised Three-Dimensional Point Clouds from Near-Monostatic Laser Scanners Using Covariance Analysis. In: Vosselman, G., Brenner, C. (Eds.) Laserscanning 2005. International Archives of Photogrammetry, Remote Sensing and Spatial Information Sciences 36 (Part 3-W19), pp. 7-12.

Brenner, C., Haala, N. Fritsch, D., 2001. Towards fully automated 3D city model generation. In: Baltsavias, E., Grün, A., van Gool, L. (Eds) Proceedings of the 3rd International Workshop on Automatic Extraction of Man-Made Objects from Aerial and Space Images, pp. 47-56.

Geibel, R., Stilla, U., 2000. Segmentation of Laser-altimeter data for building reconstruction: Comparison of different procedures. International Archives of Photogrammetry and Remote Sensing 33 (Part B3), pp. 326-334.

Gross, H., Thoennessen, U., v. Hansen, W., 2005. 3D Modeling of Urban Structures. In: Stilla, U., Rottensteiner, F., Hinz, S. (Eds) Joint Workshop of ISPRS/DAGM Object Extraction for 3D City Models, Road Databases, and Traffic Monitoring CMRT05, International Archives of Photogrammetry and Remote Sensing 36 (Part 3/W24), pp. 137-142.

Gross, H., Thoennessen, U., 2006. Extraction of Lines from Laser Point Clouds. In: Förstner, W., Steffen, R. (Eds) Symposium of ISPRS Commission III: Photogrammetric Computer Vision PCV06. International Archives of Photogrammetry, Remote Sensing and Spatial Information Sciences 36 (Part 3), pp. 86-91.

Höfle, B., Pfeifer, N., 2007. Correction of laser scanning intensity data: Data and model-driven approaches. ISPRS Journal of Photogrammetry and Remote Sensing 62 (6), pp. 415-433.

Hofton, M.A., Minster, J.B., Blair, J.B., 2000. Decomposition of laser altimeter waveforms. IEEE Transactions on Geoscience and Remote Sensing 38 (4), pp. 1989–1996.

Jelalian, A.W., 1992. Laser Radar Systems. Artech House, Boston, MA.

Jutzi, B., Neulist J., Stilla, U., 2005. Sub-Pixel Edge Localization Based on Laser Waveform Analysis. In: Vosselman, G., Brenner, C. (Eds.) Laserscanning 2005. International Archives of Photogrammetry, Remote Sensing and Spatial Information Sciences 36 (Part 3-W19), pp. 109-114.

Jutzi, B., Stilla, U., 2006. Range determination with waveform recording laser systems using a Wiener Filter. ISPRS Journal of Photogrammetry and Remote Sensing 61 (2), pp. 95-107.

Kamermann, G.W., 1993. Laser Radar. In: Fox, C.S. (Ed.) Active Electro-Optical Systems, The Infrared & Electro-Optical Systems Handbook. SPIE Optical Engineering Press, Michigan.
Katzenbeisser, R., 2003. Technical Note on Echo Detection. http://www.toposys.de/pdfext/Engl/echo-detec3.pdf (Accessed 30. April 2008).

Kukko A., Kaasalainen S., Litkey P., 2007. Effect of incidence angle on laser scanner intensity and surface data. Applied Optics, Vol. 47, No. 7, March 2008, pp. 986-992

Lovell, J.L., Jupp, D.L.B., Culvenor, D.S., Coops, N.C., 2003. Using airborne and ground based ranging Lidar to measure canopy structure in Australian forests. Canadian Journal of Remote Sensing 29 (5), pp. 607–622.

Lutz, E., Geist, Th., Stötter, J., 2003. Investigations of airborne laser scanning signal intensity on glacial surfaces - utilizing comprehensive laser geometry modeling and orthophoto surface modelling. In: Maas, H.-G., Vosselman, G., Streilein, A. (Eds.) International Archives of Photogrammetry, Remote Sensing and Spatial Information Sciences 36 (Part 3-W13), pp. 143-148.

Persson, Å., Söderman, U., Töpel, J., Ahlberg, S., 2005. Visualization and Analysis of Full-Waveform Airborne Laser Scanner Data. In: Vosselman, G., Brenner, C. (Eds.) Laserscanning 2005. International Archives of Photogrammetry, Remote Sensing and Spatial Information Sciences 36 (Part 3/W19), pp. 109-114.

Pfeifer, N., Dorninger, P., Haring, A., Fan, H., 2007. Investigating terrestrial laser scanning intensity data: quality and functional relations. In: Gruen, A., Kahmen, H. (Eds.) International Conference on Optical 3-D Measurement Techniques VIII, Zürich, Switzerland, ISBN 3-906467-67-8, pp. 328-337.

Reshetyuk, Y., 2006. Investigation of the Influence of Surface Reflectance on the Measurements with the Terrestrial Laser Scanner Leica HDS 3000. Zeitschrift für Geodasie, Geoinformation und Landmanagement 131 (2), pp. 96-103.

Wagner, W., Ullrich, A., Ducic, V., Melzer, T., Studnicka, N., 2006. Gaussian Decomposition and Calibration of a Novel Small-Footprint Full-Waveform Digitising Airborne Laser Scanner. ISPRS Journal of Photogrammetry and Remote Sensing, 60 (2), pp. 100-112.

West, K.F., Webb, B.N., Lersch, J.R., Pothier, S., Triscari, J.M., Iverson, A.E., 2004. Context-driven automated target detection in 3d data. In: Sadjadi, F.A. (Ed) Automatic Target Recognition XIV. Proceedings of SPIE Vol. 5426, pp. 133-143.